Implementation of the XFEM for Hydraulic Fracture Problems

Zuorong Chen*

CSIRO Earth Science & Resource Engineering, Melbourne, Australia
* Corresponding author: zuorong.chen@csiro.au

Abstract A new finite element has been implemented to incorporate the extended finite element method (XFEM) for the solution of hydraulic fracture problems. The proposed element includes the desired aspects of the XFEM so as to model crack propagation without explicit remeshing. In addition, the fluid pressure degrees of freedom have been defined on the element to describe the fluid flow within the crack and its contribution to the crack deformation. Thus the fluid flow within the crack and crack propagation are fully coupled in a natural way and are solved simultaneously. Verification of the proposed element has been conducted by comparing the finite element results with the analytical solutions available in the literature.

Keywords Hydraulic fracture, Extended finite element method, Internal pressure

1. Introduction

Hydraulic fracturing is a powerful technology for enhancing conventional petroleum production. It is playing a central role in fast growing development of unconventional gas and geothermal energy. The fully 3-D numerical simulation of the hydraulic fracturing process is of great importance to understand the complex, multiscale mechanics of hydraulic fracturing, to the efficient application of this technology, and to develop innovative, advanced hydraulic fracturing technologies for unconventional gas production. The accurate numerical simulation of hydraulic fracture growth remains a significant challenge because of the strong nonlinear coupling between the viscous flow of fluid inside the fracture and fracture propagation (a moving boundary), complicated by the need to consider interactions with existing natural fractures and with rock layers with different properties.

Great effort has been devoted to the numerical simulation of hydraulic fractures with the first 3-D modeling efforts starting in the late 1970s [1-2]. Significant progress has been made in developing 2-D and 3-D numerical hydraulic fracture models [3-15]. Boundary integral equation methods or displacement discontinuity techniques have generally been employed to investigate the propagation of simple hydraulic fractures such as penny-shaped or plane-strain fractures in a homogeneous, infinite or semi-infinite elastic medium where the appropriate fundamental solutions are available. The finite element method has been used and is particularly useful in modelling the hydraulic fracture propagation in inhomogeneous rocks which may include nonlinear mechanical properties and may be subject to complex boundary conditions. The finite element model is also able to investigate the propagation of hydraulic fractures in infinite or semi-infinite medium by using infinite elements or appropriate analytical solutions to efficiently approximate the far-field boundary [15]. However, the standard finite element model requires remeshing after every crack propagation step and the mesh has to conform exactly to the fracture geometry as the fracture propagates, and thus is computationally expensive.

By adding special enriched shape functions in conjunction with additional degrees of freedom to the standard finite element approximation within the framework of partition of unity, the extended finite element method [16-17] (XFEM) overcomes the inherent drawbacks associated with use of the conventional finite element methods and enables the crack to be represented without explicitly meshing crack surfaces, and so the crack geometry is completely independent of the mesh and remeshing is not required, allowing for the convenient simulation of the fracture propagation. The XFEM has been employed to investigate the hydraulic fracture problems [18-19].

In this paper, we explore the application of the extended finite element method to hydraulic fracture problems. By taking good advantage of the XFEM and the flexible functionality of user subroutines provided in ABAQUS [20], a user-defined 2-D quadrilateral plane strain element has been coded in Fortran to incorporate the extended finite element capabilities in 2-D hydraulic fracture problems. The user-defined element includes the desired aspects of the XFEM so as to model crack propagation without explicit remeshing. In addition, the extended fluid pressure degrees of freedom are assigned to the appropriate nodes of the proposed elements in order to describe the viscous flow of fluid inside the crack and its contribution to the coupled crack deformation.

2. Problem formulation

2.1. Problem definition

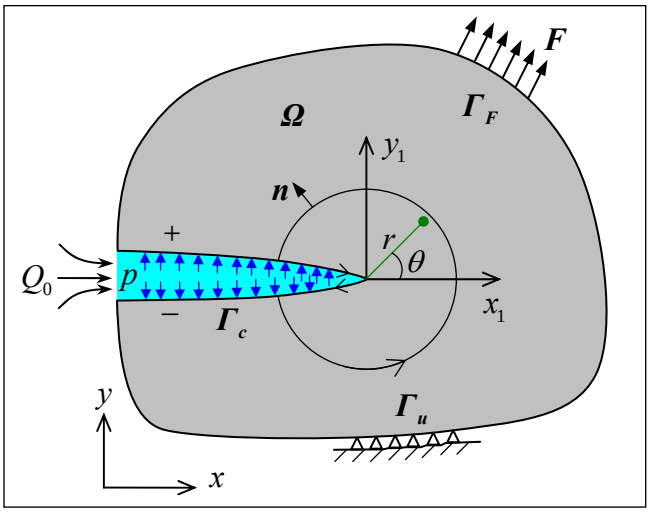

Figure 1. A two-dimensional domain containing a hydraulic fracture

Consider a two-dimensional hydraulically driven fracture Γ_c propagating in a homogeneous, isotropic, linear elastic, impermeable medium Ω under plane strain conditions, see Figure 1. The boundary of the domain consists of Γ_F on which prescribed tractions $\boldsymbol{F}$, are imposed, Γ_u on which prescribed displacements (assumed to be zero for simplicity) are imposed, and crack faces Γ_c subject to fluid pressure. The fracture propagation is driven by injection of an incompressible Newtonian fluid at constant volumetric rate Q_0 at a fixed injection point. It is assumed that the fracture propagation is quasi-static, and that the fracture is completely filled with the injected fluid, i.e., there is no lag between the fluid front and the fracture tip. The solution of the problem consists of determining the evolution of the fracture length, as well as the fracture opening, the fluid pressure, and the deformations and stresses inside the domain as functions of both position and time.

2.2 Governing equations

The stress field inside the domain, $\boldsymbol{\sigma}$, is related to the external loading $\boldsymbol{F}$ and the fluid pressure p through the equilibrium equations:

$$\begin{aligned} &\nabla \cdot \boldsymbol{\sigma} = \boldsymbol{0}, \text{ on } \Omega \\ &\boldsymbol{\sigma} \cdot \boldsymbol{n} = \boldsymbol{F}, \text{ on } \Gamma_F \\ &\boldsymbol{\sigma} \cdot \boldsymbol{n}^- = -\boldsymbol{\sigma} \cdot \boldsymbol{n}^+ = -p\boldsymbol{n}^+ = p\boldsymbol{n}^-, \text{ on } \Gamma_c \end{aligned} \tag{1}$$

where $\boldsymbol{n}$ is the unit normal vector.

The kinematic equations include the strain-displacement relationship, the prescribed displacement boundary conditions and the definition of the separation between the two surfaces of the crack. Under the assumptions of small strains and displacements, the kinematic equations read

$$\begin{aligned} &\boldsymbol{\varepsilon} = \frac{1}{2}\left(\nabla \boldsymbol{u} + (\nabla \boldsymbol{u})^{\mathrm{T}}\right) \text{ on } \Omega \\ &\boldsymbol{u} = \boldsymbol{0} \text{ on } \Gamma_u \\ &\boldsymbol{w} = \boldsymbol{u}^+ - \boldsymbol{u}^- \text{ on } \Gamma_c \end{aligned} \tag{2}$$

where $\boldsymbol{u}$ is the displacement, $\boldsymbol{w}$ is the separation between the two faces of the crack, and $\boldsymbol{\varepsilon}$ is the strain.

The stress field insider the domain is expressed in terms of the isotropic, linear elastic constitutive law as:

$$\boldsymbol{\sigma} = \boldsymbol{D} : \boldsymbol{\varepsilon} \tag{3}$$

where $\boldsymbol{D}$ is Hooke's tensor.

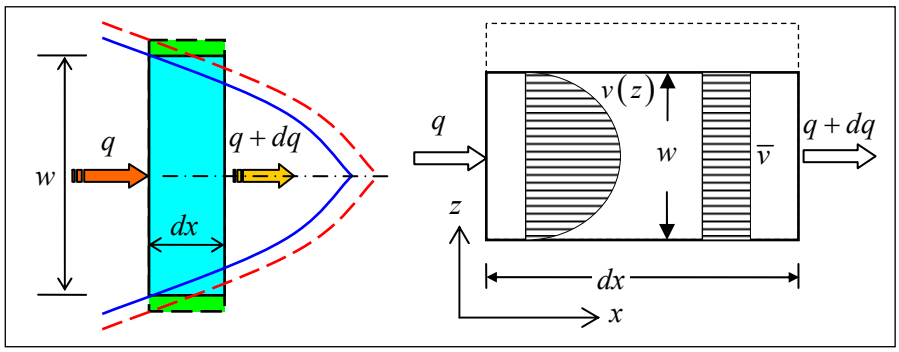

Figure 2. Fluid flow within crack

The fluid flow within the crack is modelled using lubrication theory, given by Poiseuille's law

$$q = -\frac{w^3}{12\mu}\frac{\partial p}{\partial x} \tag{4}$$

where μ is the dynamic viscosity of the fracturing fluid, q, the flow rate inside the crack per unit extend of the crack in the direction of x, is equal to the average velocity $\bar{v}$ times the crack opening w (see Figure 2), i.e.,

$$q(x) = \bar{v}(x)w(x) \tag{5}$$

The fracturing fluid is considered to be incompressible, so the mass conservation equation for the fluid may be expressed as

$$\frac{\partial w}{\partial t} + \frac{\partial q}{\partial x} + g = 0 \tag{6}$$

where the flux discontinuity $g(\boldsymbol{x})$ is taken as positive if fluid is leaving the fracture. It can be interpreted as a source density outside the fracture, which accounts for fluid exchange between the fracture and the surrounding medium (e.g. porous rock).

Substituting of Eq. (4) into Eq. (6) leads to the governing equation for the fluid flow within the fracture

$$\frac{\partial w}{\partial t}-\frac{\partial}{\partial x}\left(k\frac{\partial p}{\partial x}\right)+g=0 \tag{7}$$

where $k=w^3/12\mu$ is the permeability. The general form of the governing equation (Eq. (7)) may be expressed as

$$\dot{w}-\nabla^{\mathrm{T}}\left(\boldsymbol{k}\nabla p\right)+g=0 \tag{8}$$

where $\boldsymbol{k}$ is the permeability tensor.

According to linear elastic fracture mechanics, the criterion that the fracture propagates continuously in mobile equilibrium (quasi-static) takes the form

$$K_{\mathrm{I}}=K_{\mathrm{Ic}} \tag{9}$$

where K_{I} is the mode I stress intensity factor and K_{Ic} the material fracture toughness.

At the inlet, the fluid flux is equal to the injection rate, i.e.,

$$q\big|_{\mathrm{inlet}}=Q_0 \tag{10}$$

At the tip, the boundary conditions are given by the zero fracture opening and zero flow conditions,

$$w\big|_{\mathrm{tip}}=q\big|_{\mathrm{tip}}=0 \tag{11}$$

The above equations constitute the complete formulation that can be used to predict the evolution of the hydraulic fracture.

3. Weak form and FEM discretization

The weak form of the equilibrium equation is given by

$$\int_\Omega \delta\boldsymbol{\varepsilon}^{\mathrm{T}}\boldsymbol{\sigma}d\Omega-\int_\Omega \delta\boldsymbol{u}^{\mathrm{T}}\boldsymbol{b}d\Omega-\int_{\Gamma_t}\delta\boldsymbol{u}^{\mathrm{T}}\boldsymbol{t}d\Gamma-\left(\int_{\Gamma_c^+}\delta\boldsymbol{u}_c^{+\mathrm{T}}\boldsymbol{p}_c^+d\Gamma+\int_{\Gamma_c^-}\delta\boldsymbol{u}_c^{-\mathrm{T}}\boldsymbol{p}_c^-d\Gamma\right)=0 \tag{12}$$

where $\boldsymbol{b}$ is the body force, $\boldsymbol{t}$ is the applied traction on the boundary $\boldsymbol{\Gamma}_t$, $\delta\boldsymbol{u}$ is an arbitrary virtual displacement and $\delta\boldsymbol{\varepsilon}$ is the corresponding virtual strain, which is related to $\delta\boldsymbol{u}$ through the strain operator $\boldsymbol{S}$ as $\delta\boldsymbol{\varepsilon}=\boldsymbol{S}\delta\boldsymbol{u}$.

For the fluid pressure on the crack surfaces, we define

$$\boldsymbol{p}=\boldsymbol{p}_c^+=-\boldsymbol{p}_c^-=p\boldsymbol{n}_c=p\boldsymbol{n}_c^-=-p\boldsymbol{n}_c^+. \tag{13}$$

The crack opening displacement $\boldsymbol{w}$ is given by

$$w=\boldsymbol{n}_c^{\mathrm{T}}\cdot\left(\boldsymbol{u}_c^+-\boldsymbol{u}_c^-\right),\ \text{or}\ \ \boldsymbol{w}=\boldsymbol{n}_c\cdot\left(\boldsymbol{u}_c^+-\boldsymbol{u}_c^-\right)\cdot\boldsymbol{n}_c. \tag{14}$$

Then the weak from of the equilibrium equation can be expressed in a more compact form as

$$\int_\Omega \delta\boldsymbol{\varepsilon}^{\mathrm{T}}\boldsymbol{\sigma}d\Omega-\int_\Omega \delta\boldsymbol{u}^{\mathrm{T}}\boldsymbol{b}d\Omega-\int_{\Gamma_t}\delta\boldsymbol{u}^{\mathrm{T}}\boldsymbol{t}d\Gamma-\int_{\Gamma_c}\delta\boldsymbol{w}^{\mathrm{T}}\boldsymbol{p}d\Gamma=0. \tag{15}$$

The weak form of the governing equation for the fluid flow within the fracture can be written as

$$\int_{\Gamma_c}\delta p^{\mathrm{T}}\left(\partial\dot{w}-\nabla^{\mathrm{T}}\boldsymbol{k}\nabla p+g\right)d\Gamma=0 \tag{16}$$

which, after integration by parts and substitution of the boundary conditions describe above, yields

$$\int_{\Gamma_c}\delta p^{\mathrm{T}}\partial\dot{w}d\Gamma+\int_{\Gamma_c}\nabla^{\mathrm{T}}\left(\delta p\right)\boldsymbol{k}\nabla pd\Gamma+\int_{\Omega_c}\delta p^{\mathrm{T}}gd\Gamma=0 \tag{17}$$

Consider the coupled problem discretized in the standard (displacement) manner with the displacement vector $\boldsymbol{u}$ approximated as

$$\boldsymbol{u} \approx \hat{\boldsymbol{u}} = \sum_{i=1}^{n} \boldsymbol{N}_i^u \boldsymbol{u}_i = \boldsymbol{N}^u \tilde{\boldsymbol{u}}, \quad \delta \boldsymbol{u} \approx \boldsymbol{N}^u \delta \tilde{\boldsymbol{u}} \tag{18}$$

and the fluid pressure p similarly approximated by

$$p \approx \hat{p} = \sum_{i=1}^{n} N_i^p p_i = \boldsymbol{N}^p \tilde{\boldsymbol{p}}, \quad \delta p \approx \boldsymbol{N}^p \delta \tilde{\boldsymbol{p}} \tag{19}$$

where $\boldsymbol{u}_i$ and p_i are the nodal displacement and pressure, $\boldsymbol{N}_i^u$ and N_i^p are corresponding nodal displacement and fluid pressure shape functions.

The crack opening displacement $\boldsymbol{w}$ is approximated by

$$\boldsymbol{w} \approx \hat{\boldsymbol{w}} = \sum_{i=1}^{n} \boldsymbol{N}_i^w \boldsymbol{u}_i = \boldsymbol{N}^w \tilde{\boldsymbol{u}}, \quad \delta \boldsymbol{w} \approx \boldsymbol{N}^w \delta \tilde{\boldsymbol{u}} \tag{20}$$

where $\boldsymbol{N}_i^w$ are the appropriate crack opening displacement shape function. It will be shown later that the shape function $\boldsymbol{N}_i^w$ can be expressed in terms of the displacement shape functions $\boldsymbol{N}_i^u$ according to the relationship Eq. (14).

Substitution of the displacement and pressure approximations (Eqs. (18) - (20)) and the constitutive equation (Eq. (3)) into Eq. (15) yields a system of algebraic equations for the discrete structural problem

$$\boldsymbol{K}\tilde{\boldsymbol{u}} - \boldsymbol{Q}\tilde{\boldsymbol{p}} - \boldsymbol{f}^u = \boldsymbol{0} \tag{21}$$

where

$$\boldsymbol{K} = \int_\Omega \boldsymbol{B}^{\mathrm{T}} \boldsymbol{D} \boldsymbol{B} d\Omega, \quad \boldsymbol{f}^u = \int_\Omega \left(\boldsymbol{N}^u\right)^{\mathrm{T}} \boldsymbol{b} d\Omega + \int_{\Gamma_t} \left(\boldsymbol{N}^u\right)^{\mathrm{T}} \boldsymbol{t} d\Gamma, \quad \boldsymbol{Q} = \int_{\Gamma_c} \left(\boldsymbol{N}^w\right)^{\mathrm{T}} \boldsymbol{n} \boldsymbol{N}^p d\Gamma \tag{22}$$

By substituting Eqs. (19) and (20) into Eq. (17), the standard discretization applied to the weak form of the fluid flow equation leads to a system of algebraic equations for the discrete fluid flow problem

$$\boldsymbol{C}\dot{\tilde{\boldsymbol{u}}} + \boldsymbol{H}\tilde{\boldsymbol{p}} - \boldsymbol{f}^p = \boldsymbol{0} \tag{23}$$

where

$$\boldsymbol{C} = \boldsymbol{Q}^{\mathrm{T}} = \int_{\Gamma_c} \left(\boldsymbol{N}^p\right)^{\mathrm{T}} \boldsymbol{n}^{\mathrm{T}} \boldsymbol{N}^w d\Gamma, \quad \boldsymbol{H} = \int_{\Gamma_c} \left(\nabla \boldsymbol{N}^p\right)^{\mathrm{T}} \boldsymbol{k} \nabla \boldsymbol{N}^p d\Gamma, \quad \boldsymbol{f}^p = -\int_{\Gamma_c} \left(\boldsymbol{N}^p\right)^{\mathrm{T}} g d\Gamma \tag{24}$$

Then, the discrete governing equations for the coupled fluid-fracture problem can be expressed in matrix form as:

$$\begin{bmatrix} \boldsymbol{0} & \boldsymbol{0} \\ \boldsymbol{C} & \boldsymbol{0} \end{bmatrix} \begin{pmatrix} \dot{\tilde{\boldsymbol{u}}} \\ \dot{\tilde{\boldsymbol{p}}} \end{pmatrix} + \begin{bmatrix} \boldsymbol{K} & \boldsymbol{-Q} \\ \boldsymbol{0} & \boldsymbol{H} \end{bmatrix} \begin{pmatrix} \tilde{\boldsymbol{u}} \\ \tilde{\boldsymbol{p}} \end{pmatrix} = \begin{pmatrix} \boldsymbol{f}^u \\ \boldsymbol{f}^p \end{pmatrix} \tag{25}$$

The above equations form the basis for the construction of a finite element which couples the fluid flow within the crack and crack propagation.

4. The extended finite element method and element implementation

4.1 Extended finite element approximation

By adding special enriched shape functions in conjunction with additional degrees of freedom to the standard finite element approximation within the framework of partition of unity, the extended finite element method (XFEM) [16-17] overcomes the inherent drawbacks associated with use of the

conventional finite element methods and enables the crack to be represented without explicitly meshing crack surfaces, and so the crack geometry is completely independent of the mesh and remeshing is not required, allowing for the convenient simulation of the fracture propagation.

The XFEM approximation of the displacement field for the crack problem can be expressed as [17]

$$\mathbf{u}(\mathbf{x}) = \sum_{I\in N} \boldsymbol{N}_I(\mathbf{x})\mathbf{u}_I + \sum_{I\in N_{cr}} \tilde{\boldsymbol{N}}_I(\mathbf{x})\left(H(\mathbf{x}) - H(\mathbf{x}_I)\right)\mathbf{a}_I + \sum_{I\in N_{tip}} \tilde{\boldsymbol{N}}_I(\mathbf{x})\sum_{l=1}^{4}\left(B^{(l)}(r,\theta) - B^{(l)}(r_I,\theta_I)\right)\mathbf{b}_I^{(l)} \tag{26}$$

where N is the set of all nodes in the mesh, N_{cr} the set of nodes whose support are bisected by the crack surface Γ_c, N_{tip} the set of nodes whose support are partially cut by the crack surface, $\boldsymbol{N}_I(\mathbf{x})$ and $\tilde{\boldsymbol{N}}_I(\mathbf{x})$ are the standard finite element shape functions, $\mathbf{u}_I$ are displacement nodal degrees of freedom, $\mathbf{a}_I$ and $\mathbf{b}_I^{(l)}$ are additional degrees of freedom for the displacement, and $H(\mathbf{x})$ and $B^{(l)}(r,\theta)$ are the appropriate enrichment basis functions which are localized by $\tilde{\boldsymbol{N}}_I(\mathbf{x})$. The shape function $\tilde{\boldsymbol{N}}_I(\mathbf{x})$ can differ from $\boldsymbol{N}_I(\mathbf{x})$.

The discontinuity in the displacement field given by a crack Γ_c can be represented by the generalized Heaviside step function

$$H(\mathbf{x}) = H\left(d(\mathbf{x})\right) = sign\left(d(\mathbf{x})\right) = \begin{cases} 1 & d(\mathbf{x}) \geq 0 \\ -1 & d(\mathbf{x}) < 0 \end{cases} \tag{27}$$

where $d(\mathbf{x})$ is the signed distance of the point $\mathbf{x}$ to Γ_c.

The enrichment basis functions $B^{(l)}(r,\theta)$ are required to model the displacement around the crack tip, which are generally chosen as a basis that approximately spans the two-dimensional plane strain asymptotic crack tip fields in the linear elastic fracture mechanics:

$$\left\{B^{(l)}\right\}_{l=1}^{4} = \sqrt{r}\left\{\sin(\theta/2) \quad \cos(\theta/2) \quad \sin(\theta/2)\sin(\theta) \quad \cos(\theta/2)\sin(\theta)\right\} \tag{28}$$

where (r,θ) are the local polar coordinates at the crack tip. The first function in Eq. (28), $\sin(\theta/2)$, is discontinuous across the crack faces $(\theta = \pm\pi)$, so the Heaviside enrichment in Eq. (26) can be removed in the displacement field approximation of the elements which are partially cut by the crack surface.

According to Eq. (26), the displacement discontinuity between the two surfaces of the crack can be obtained as

$$\mathbf{w}(\mathbf{x}) = \mathbf{u}^{(+)}(\mathbf{x}) - \mathbf{u}^{(-)}(\mathbf{x}) = 2\sum_{I\in N_{cr}} \tilde{\boldsymbol{N}}_I(\mathbf{x})\mathbf{a}_I + 2\sum_{I\in N_{tip}} \tilde{\boldsymbol{N}}_I(\mathbf{x})B^{(1)}(r,\pi)\mathbf{b}_I^{(1)} \qquad \boldsymbol{x}\in\Gamma_c \tag{29}$$

Combination of Eqs. (29) and (20) enables determining the shape function $\boldsymbol{N}^w$.

The fluid pressure field within the crack is approximated by

$$p(\mathbf{x}) = \sum_{I\in N_{cr}} N_I^p(\mathbf{x})\,p_I \qquad \boldsymbol{x}\in\Gamma_c \tag{30}$$

where $N_I^p(\mathbf{x})$ are the standard finite element shape functions. In some cases, it can also be chosen as a special function so as to allow for the pressure singularity at the crack tip and the associated near-tip asymptotic fracture opening associated with a zero-lag viscosity dominated regime in a

hydraulic fracture [18].

4.2 Element implementation

As shown in Figure 3, the two-dimensional 4-node plane strain channel and tip elements have been constructed for the hydraulic fracture problem. Each node has the standard displacement degrees of freedom $\mathbf{u}_I$. The additional degree of freedom $\mathbf{a}_I$ and $\mathbf{b}_I^{(l)}$ are assigned to the four nodes of channel and tip elements, respectively. In addition, the virtual degree of freedom of fluid pressure has been assigned to nodes 3 and 4 so as to represent the internal fluid pressure within the crack. It should be pointed out that nodes 3 and 4 physically do not have fluid pressure degrees of freedom because here the fluid flow is confined within the crack. So the integral calculation of the related element matrixes and equivalent nodal forces (e.g. Eq. (24)) must be correctly carried out along the true crack path within the element.

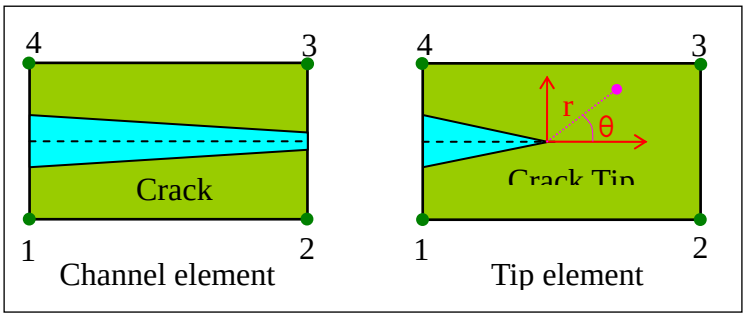

Figure 3. 2-D 4-node plane strain hydraulic fracture elements

So, the active degrees of freedom for the channel element are

$$\hat{\mathbf{u}}^{\mathbf{e}} = \{ \underbrace{u_1^x \quad u_1^y \quad u_2^x \quad u_2^y \quad u_3^x \quad u_3^y \quad u_4^x \quad u_4^y}_{\text{Standard}} \quad \underbrace{a_1^x \quad a_1^y \quad a_2^x \quad a_2^y \quad a_3^x \quad a_3^y \quad a_4^x \quad a_4^y}_{\text{Heaviside Enriched}} \quad \underbrace{p_3 \quad p_4}_{\text{Coupled}} \}_{18}^{\mathrm{T}} \tag{31}$$

and for the tip element the Heaviside enriched degrees of freedom $\mathbf{a}_I$ need to be replaced by the crack tip field enriched degrees of freedom $\mathbf{b}_I^{(l)}$.

According to the element connectivity and the arrangement of nodal degrees of freedom, the bilinear shape functions are used to approximate the displacement field, and the linear shaped functions are used to approximate the fluid pressure field.

Gauss quadrature is used to calculate the system matrix and equivalent nodal force. Since the discontinuous enrichment functions are introduced in approximating the displacement field, integration of discontinuous functions is needed when computing the element stiffness matrix and equivalent nodal force. In order to ensure the integral accuracy, it is necessary to modify the quadrature routine. Both the channel and tip elements are partitioned by the crack surface into two quadrature sub-cells where the integrands are continuous and differentiable. Then Gauss integration is carried out by a loop over the sub-cells to obtain an accurate integration result.

Due to the flexibility, the user subroutine of UEL provided in the finite element package ABAQUS [20] has been employed in implementing the proposed elements in Fortran code. The main purpose of UEL is to provide the element stiffness matrix as well as the right hand side residual vector, as need in a context of solving the discrete system of equations.

5. Numerical Examples

The proposed user element together with the structural elements provided in the ABAQUS element library are used to establish a finite element model to investigate a plane strain hydraulic fracture problem in an infinite impermeable elastic medium. The far-field boundary conditions are modelled by using infinite elements. The initial testing of this new element formulation involves using boundary value problems of an imposed fluid pressure and an imposed fracture opening. These problems are used to test for both of the two limiting cases of a toughness-dominated and viscosity-dominated plane-strain hydraulic fracture for which the analytical solutions are available in the literature [21].

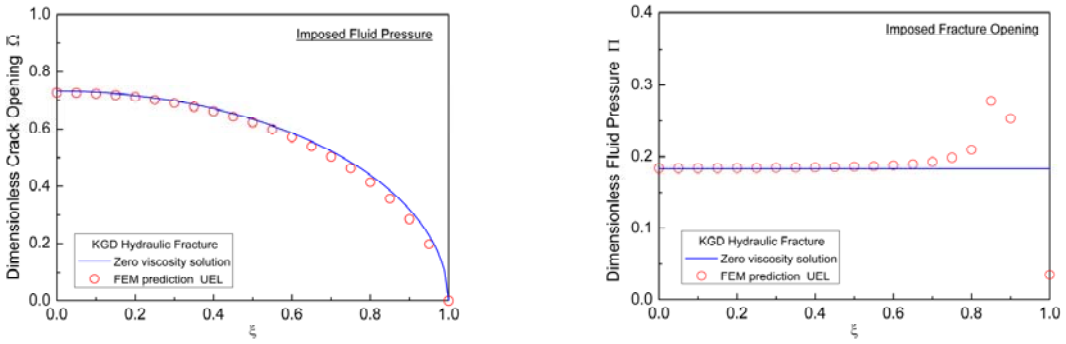

(a) (b)

Figure 4. Zero-viscosity case: (a) Imposed pressure; and (b) Imposed opening

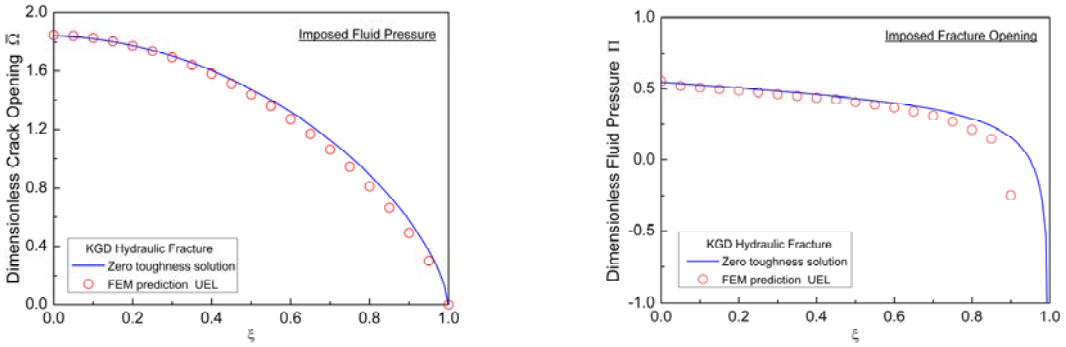

(a) (b)

Figure 5. Zero-toughness case: (a) Imposed pressure; and (b) Imposed opening

The simulation results for a plane strain toughness-dominated KGD hydraulic fracture are shown in Figure 4. The corresponding analytical solutions for the zero-viscosity case are also shown for comparison. The crack opening is obtained by imposing a given pressure calculated according to the analytical solution [21] on the crack surface of the finite element model. While the fluid pressure is obtained by applying an opening profile calculated from the analytical solution [21] to the crack surface of the finite element model. The results for the zero-toughness case are shown in Figure 5. Only twenty channel elements in total are meshed along the crack length in the finite element model.

It can be seen that the XFEM predictions generally compare well with the analytical solutions for crack openings, while for the fluid pressure the XFEM predictions differ from the analytical solutions at the region close to the crack tip. One main reason for the deviation of the predicted fluid pressure from the analytical solutions near the tip is likely to be because the user-defined element is assumed to be cut through by the crack and no tip element is included in the finite

element model. Another reason could be that a static fracture rather than a propagating fracture is simulated here. Improved prediction can be expected with including the crack tip element that captures the crack tip singularity correctly.

Figure 6 shows the stress field and crack opening profile of a center-cracked tension plate subjected to uniform tensile stress of 1.0 MPa. The width of the plate is 40 m and the half length of the crack is 5 m. The corrected stress intensity factor [22] is K_I=3.995 MPa$\sqrt{\text{m}}$. The calculation of the stress intensity factors is performed with the domain form of interaction integral. The computed stress intensity factors are K_I=3.954 MPa$\sqrt{\text{m}}$, and K_{II}=3.8×10^{-8} MPa$\sqrt{\text{m}}$.

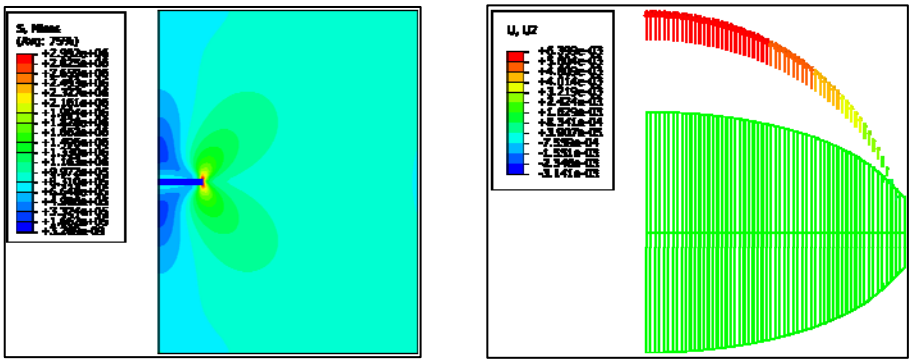

Figure 6. Stress and crack opening profile of a center-cracked tension plate

6. Summary

The application of the extended finite element method to the hydraulic fracture problems has been presented. The discrete governing equations for the coupled fluid-fracture problem have been derived. A user element based on the XFEM has been implemented in ABAQUS, which includes the desired aspects of the XFEM so as to model crack propagation without explicit remeshing. In addition, the fluid pressure degrees of freedom have been introduced and assigned to the appropriate nodes of the proposed element to describe the fluid flow within the crack and its contribution to the crack deformation. Verification of the user-defined element has been made by comparing the FEM predictions with the analytical solutions available in the literature. The preliminary result presented here is a first attempt to the promising application of the XFEM to the hydraulic fracture simulation.

Acknowledgements

The author would like to thank Dr. Rob Jeffrey for the support of this work. Furthermore, the author thanks CESRE for support and for granting permission to publish.

References

[1] R. J. Clifton, A. S. Abou-Sayed, On the computation of the 3-D geometry of hydraulic fractures, in Proceedings of the SPE Symposium on Low Permeability Gas Reservoir, Denver, Richardson, 1979, pp. 307-313.

[2] A. Settari, M. P. Cleary, 3-D simulation of hydraulic fracturing, Journal of Petroleum Technology, 36(1984) 1177-1190.

[3] L. Vandamme, J. H. Curran, A 3-D hydraulic fracturing simulator, International Journal for Numerical Methods in Engineering, 28(1989) 909-927.

[4] S. H. Advani, T. S. Lee, J. K. Lee, 3-D modeling of hydraulic fractures in layered media .1. Finite-element formulations, Journal of Energy Resources Technology-Transactions of the ASME, 112(1990) 1-9.

[5] P. Valko, M. J. Economides, Propagation of hydraulically induced fractures - a continuum damage mechanics approach, International Journal of Rock Mechanics and Mining Sciences & Geomechanics, 31(1994) 221-229.

[6] S. Ouyang, G. F. Carey, C. H. Yew, An adaptive finite element scheme for hydraulic fracturing with proppant transport, International Journal for Numerical Methods in Fluids, 24(1997) 645-670.

[7] P. Papanastasiou, An efficient algorithm for propagating fluid-driven fractures, Computational Mechanics, 24(1999) 258-267.

[8] X. Zhang, E. Detournay, R. Jeffrey, Propagation of a penny-shaped hydraulic fracture parallel to the free-surface of an elastic half-space, International Journal of Fracture, 115(2002) 125-158.

[9] J. Adachi, E. Siebrits, A. Peirce, J. Desroches, Computer simulation of hydraulic fractures, International Journal of Rock Mechanics and Mining Sciences, 44(2007) 739-757.

[10] B. Lecamplon, E. Detournay, An implicit algorithm for the propagation of a hydraulic fracture with a fluid lag, Computer Methods in Applied Mechanics and Engineering, 196(2007) 4863-4880.

[11] A. Peirce, E. Detournay, An implicit level set method for modeling hydraulically driven fractures, Computer Methods in Applied Mechanics and Engineering, 197(2008) 2858-2885.

[12] Z. R. Chen, A. P. Bunger, X. Zhang, R. G. Jeffrey, Cohesive zone finite element-based modeling of hydraulic fractures, Acta Mechanica Solida Sinica, 22(2009) 443-452.

[13] R. H. Dean, J. H. Schmidt, Hydraulic-fracture predictions with a fully coupled geomechanical reservoir simulator, SPE Journal, 14(2009) 707-714.

[14] B. Carrier, S. Granet, Numerical modeling of hydraulic fracture problem in permeable medium using cohesive zone model, Engineering Fracture Mechanics, 79(2012) 312-328.

[15] Z. R. Chen, Finite element modelling of viscosity-dominated hydraulic fractures, Journal of Petroleum Science and Engineering, 88-89(2012) 136-144.

[16] T. Belytschko, T. Black, Elastic crack growth in finite elements with minimal remeshing, International Journal for Numerical Methods in Engineering, 45(1999) 601-620.

[17] N. Moes, J. Dolbow, T. Belytschko, A finite element method for crack growth without remeshing, International Journal for Numerical Methods in Engineering, 46(1999) 131-150.

[18] B. Lecampion, An extended finite element method for hydraulic fracture problems, Communications in Numerical Methods in Engineering, 25(2009) 121-133.

[19] A. Dahi-Taleghani, J. E. Olson, Numerical modeling of multistranded-hydraulic-fracture propagation: Accounting for the interaction between induced and natural fractures, SPE Journal, 16(2011) 575-581.

[20] ABAQUS, Abaqus documentation version 6.11-1, 2011.

[21] E. Detournay, Propagation regimes of fluid-driven fractures in impermeable rocks, International Journal of Geomechanics, 4(2004) 35-45.

[22] H. L. Ewalds, R. J. H. Wanhill, Fracture mechanics. New York: Edward Arnold, 1989.